Available online at www.sciencedirect.com
ScienceDirect
Biochimica et Biophysica Acta 1777 (2008) 277–284
Biochimica et Biophysica Acta
BBA
www.elsevier.com/locate/bbabio

Electrostatic control of proton pumping in cytochrome *c* oxidase

Elisa Fadda *, Ching-Hsing Yu, Régis Pomès *

Molecular Structure and Function, Hospital for Sick Children, Toronto, Ontario, Canada
Department of Biochemistry, University of Toronto, Ontario, Canada

Received 24 September 2007; received in revised form 19 November 2007; accepted 21 November 2007
Available online 14 December 2007

Abstract

As part of the mitochondrial respiratory chain, cytochrome *c* oxidase utilizes the energy produced by the reduction of O_2 to water to fuel vectorial proton transport. The mechanism coupling proton pumping to redox chemistry is unknown. Recent advances have provided evidence that each of the four observable transitions in the complex catalytic cycle consists of a similar sequence of events. However, the physico-chemical basis underlying this recurring sequence has not been identified. We identify this recurring pattern based on a comprehensive model of the catalytic cycle derived from the analysis of oxygen chemistry and available experimental evidence. The catalytic cycle involves the periodic repetition of a sequence of three states differing in the spatial distribution of charge in the active site: [0|1], [1|0], and [1|1], where the total charge of *heme a* and the binuclear center appears on the left and on the right, respectively. This sequence recurs four times per turnover despite differences in the redox chemistry. This model leads to a simple, robust, and reproducible sequence of electron and proton transfer steps and rationalizes the pumping mechanism in terms of electrostatic coupling of proton translocation to redox chemistry. Continuum electrostatic calculations support the proposed mechanism and suggest an electrostatic origin for the decoupled and inactive phenotypes of ionic mutants in the principal proton-uptake pathway.

Keywords: Cytochrome *c* oxidase; Vectorial proton transport; Redox-coupled proton transport; Proton-pumping mechanism; Binuclear center; Continuum electrostatics

1. Introduction

Cytochrome *c* oxidase (C*c*O) is the fourth enzyme complex in the mitochondrial respiratory chain. As a self-reliant proton pump, it fuels vectorial proton transport by reducing O_2 to water (For recent reviews see Refs. [1–3]). This redox reaction takes place in a binuclear center (BNC) (see Fig. 1), which includes a Cu center (Cu_B) and a high-spin Fe-heme (*heme a3*), and it is carried out in a stepwise manner. Throughout the catalytic cycle, four electrons are obtained from the reduction of a bimetallic Cu center, Cu_A, by cytochrome *c*. These electrons are subsequently transferred from Cu_A to a low-spin heme complex (*heme a*; see Fig. 1). Eight protons are taken from the matrix side (N-side) of the mitochondrial membrane and translocated to the active site through two distinct pathways, the D-channel and the K-channel, which are named from conserved Asp and Lys residues (D132 and K362 in *Rhodobacter sphaeroides* C*c*O), respectively [1–3]. Four of these eight protons are consumed in the redox reaction, while the other four are translocated via the exit pathway towards the cytoplasmic side of the membrane, with an average stoichiometry of one proton pumped per electron consumed by the redox reaction [4]. At least six of the eight protons appear to be translocated to the active site through the D-channel [5,6]. A highly-conserved Glu (E286 in *R. sphaeroides* C*c*O) located at the bottleneck separating the D-channel from the active site (see Fig. 1) plays an essential role in the catalytic activity [7,8]. E286 is thought to be connected directly to the BNC and to the exit pathway via chains of hydrogen-bonded water molecules acting as proton translocation pathways [9–11]. E286 delivers chemical protons directly to the BNC whereas vectorial protons are translocated to a proton loading site (PLS) before being released to the exit pathway [12]. Although the identity of the PLS is unknown, redox-coupled proton pumping implies that it is located near the active site; recent studies suggest that the basis of the proton exit pathway lies above the hemes [13,14].

Abbreviations: C*c*O, cytochrome *c* oxidase; BNC, binuclear center; PLS, proton loading site

* Corresponding authors. Molecular Structure and Function, The Hospital for Sick Children, Toronto, Ontario, Canada M5G 1X8. Tel.: +1 416 813 5686; fax: +1 416 813 5022.
E-mail addresses: efadda@sickkids.ca (E. Fadda), pomes@sickkids.ca (R. Pomès).

0005-2728/$ - see front matter © 2007 Elsevier B.V. All rights reserved.
doi:10.1016/j.bbabio.2007.11.010

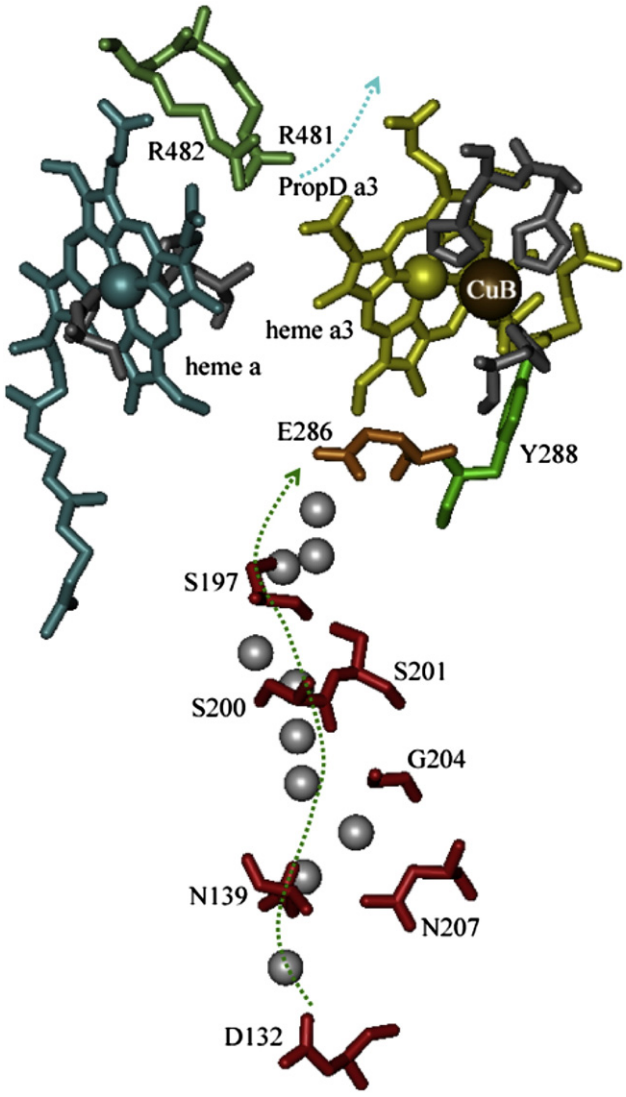

Fig. 1. Active site and D-channel of cytochrome *c* oxidase from *R. sphaeroides* (PDB ID 1M56, Ref. [36]). Key active-site residues and cofactors include *heme a3* (yellow), Cu_B (tan) with its three ligated histidines (gray), Y288 (green), E286 (orange), R481 and R482 (lime), *heme a* (cyan), H421, and H102 (gray). A light-blue arrow indicates a putative proton exit pathway starting at the R481-PropD salt-link. A green arrow connects D132 at the entrance to E286 at the top of the D-channel, with intervening residues in red and crystallographic water in white.

Numerous models of the catalytic mechanism of C*c*O have been proposed over the years [15–19]. Despite their many differences, they concur in identifying five distinct catalytic states, P, F, O, E, and R, named after the redox chemistry taking place in the BNC. Oxygen reduction is achieved step by step in the four transitions, P→F, F→O, O→E, and E→R, each of which is coupled to proton uptake from the N-side of the membrane and likely also coupled to proton pumping [2,12,20]. However, the mechanism coupling redox chemistry and proton pumping has remained elusive. Recent work by several research groups suggests that the catalytic cycle hinges on the four-fold repetition of a specific sequence of events, which account for the four electron and four protons consumed by the redox chemistry, and for the four proton pumped [2,15,18,21,22]. However, the recurring pattern characterizing this sequence of events has not been identified.

Here we build upon this emerging mechanism by proposing a simple unifying principle whereby vectorial proton movement is electrostatically coupled to redox activity by periodic fluctuations in the distribution of charge in the active site of the enzyme. Other mechanistic models based on electrostatic coupling have been proposed in the past [11,15,18,19]. The central and distinctive feature of our proposal is that even though the redox reaction itself is complex and not periodic, coupling of electron and proton movement is achieved in a simple, reproducible, and robust fashion by breaking down the catalytic cycle into four identical subcycles. In each of these subcycles, the electrostatic field in the active site acts as a three-state pendulum resulting in the consumption of one electron and one proton, and the pumping of one proton.

2. Proposed catalytic mechanism

The redox chemistry taking place in the active site of C*c*O produces only three distinct "electrostatic states". We define these states on the basis of their electrostatic charge, which takes into account only the charge of residues and cofactors in the C*c*O active site whose redox or protonation state is known to change along the catalytic cycle: Fe-porphyrin of *heme a* and of *heme a3*, Cu_B, Y288 cross-linked to H284 of Cu_B, and all intermediate products of the redox reaction. Throughout the catalytic cycle, the charges of these residues and cofactors add up to either +1 or +2. We identify a sequence of three states, which repeats itself identically four times per turnover. We write this sequence as [0|1], [1|0], and [1|1], where the total charges of *heme a* and of the BNC are shown within brackets on the left and on the right, respectively.

The basic structure of the mechanism that we propose is very simple. Each of the four observable transitions (P→F, F→O, O→E, and E→R) encompasses the same sequence of three states:

(1) In the [0|1] state, the proton loading site (PLS) is reloaded and *heme a* reduces the BNC, leading to a [1|0] state.
(2) In the [1|0] state, a substrate proton is delivered to the BNC, producing a [1|1] state.
(3) In the [1|1] state, a pumped proton is released from the PLS to the exit pathway. Reduction of *heme a* by Cu_A generates another [0|1] state and the sequence resumes.

The four-fold repetition of this sequence accounts for all four electrons, all four protons consumed in the oxygen reduction, and all four protons pumped per turnover.

A schematic depiction of our proposed mechanism is shown in Fig. 2. The catalytic cycle starts from a mixed-valence state, A_{MV}, where the BNC is fully reduced and *heme a* is formally oxidized. The charge distribution in this catalytic state is [1|1]. Here O_2 is rapidly reduced *in situ* by four electrons [23,24]. Two electrons are provided by *heme a3* [Fe_{a3}(II)→Fe_{a3}(IV)], one by Cu_B [Cu_B(I)→Cu_B(II)] and the fourth electron is

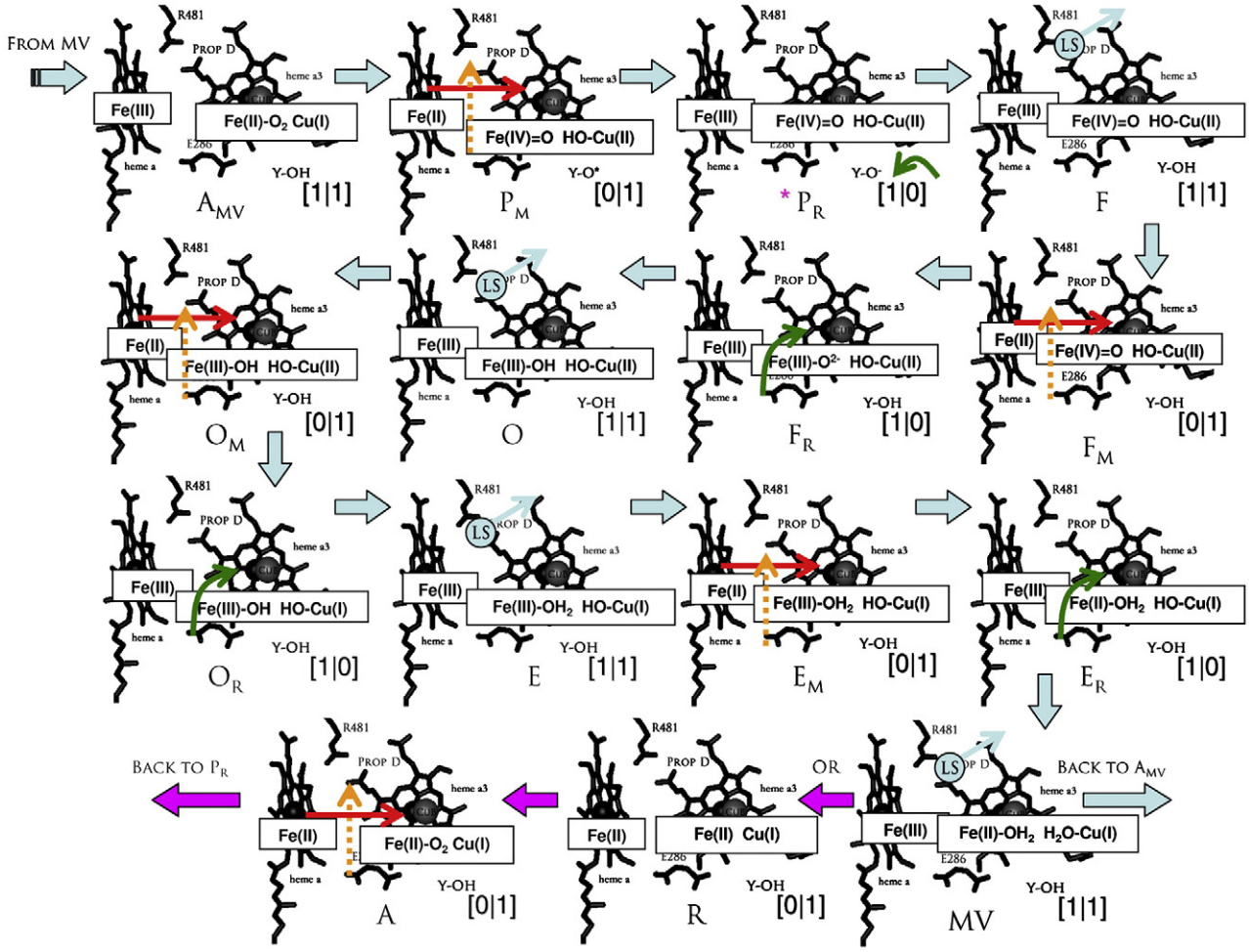

Fig. 2. Proposed catalytic mechanism. Thick light-blue arrows indicate the path through the sequence of catalytic steps. Thin red arrows indicate electron transfer from *heme a* to the BNC. Thin green arrows indicate transfer of substrate protons to the BNC. Dashed orange arrows indicate proton transfer from E286 to the PLS (pumped protons). The thick purple arrows following the MV state indicate an alternative route followed in case *heme a* is reduced when O_2 binds the BNC, in which case the cycle continues directly to the P_R state (purple asterisk).

supplied by a tyrosine residue, Y288. The latter also provides the proton necessary to break the O_2 double bond and is converted into a neutral tyrosyl radical [24]. The catalytic state reached at this point is commonly referred to as P_M [2], where this label defines only the BNC redox state. Here we extend the definition of the P_M state to take into account also the redox state of *heme a*. In terms of charge distribution we define the P_M state as a [0|1] state, where the BNC has a total charge of +1 and *heme a* is fully reduced. The high electron affinity of the tyrosyl radical induces an electron transfer from *heme a* to the BNC [21] and produces a state with charge distribution [1|0]. We refer to this state as P_R. The first substrate proton is released in the P_R [1|0] state and neutralizes the tyrosinate. Since this catalytic step is not coupled to proton uptake [17], the P_R substrate proton may originate from a titratable site in the K-channel, such as highly-conserved K362, which will be reprotonated only in the second (reductive) phase of the catalysis [25]. Neutralization of the tyrosinate leads to the F [1|1] state, in which the first vectorial proton is released from the PLS to the exit pathway.

Electron transfer from Cu_A to *heme a* generates a F_M [0|1] state, in which the BNC is a fully-oxidized [Fe_{a3}(IV)=O HO–Cu_B(II)]. Internal electron transfer from *heme a* to the BNC produces an intermediate with a high proton affinity [26]. E286 releases the substrate proton to the BNC. Protonation of the BNC produces the O [1|1] state, in which the second pumping event takes place.

The third part of the catalytic cycle starts with the O_M [0|1] state. Electron transfer from *heme a* to the BNC reduces Cu_B(II)–OH to Cu_B(I)–OH [15,26]. In the O_R [1|0] state, a chemical proton is released from E286 and the first water molecule is produced. The enzyme now reaches the E [1|1] state and the third pumping event takes place. Reduction of *heme a* by Cu_A produces the E_M [0|1] state. Internal electron transfer from *heme a* completes the reduction of Fe_{a3} in the E_R [1|0] state. The fourth substrate proton is released from E286, producing the second water molecule. The last pumping event takes place in the mixed-valence (MV) [1|1] state. This step completes the catalytic cycle.

3. Electrostatic control of proton transfer

The above mechanism provides a detailed framework to understand the coupling of vectorial proton movement to oxygen reduction and supports a specific sequence of events for proton reloading of the PLS and E286. The unifying principle behind this sequence of events, and therefore for the coupling of redox and pumping activity, is the spatial distribution of charge in the active site. As shown in Fig. 3, each of the three subcycles involving proton relay through E286 (i.e., steps F through MV, see Fig. 2) is further decomposed into a sequence of seven intermediate steps numbered 1 through 7 and comprised of two electron transfer and five proton transfer steps. These charge transfer steps are as follows: 7→1, delivery of a chemical proton to the BNC from E286; 1→2 and 5→6, reprotonation of E286 from the D-channel; 2→3, proton release from the PLS; 3→4, electron delivery to *heme a*; 4→5, reloading of the PLS from E286; and 6→7, electron transfer from *heme a* to *heme a3*.

Each of the three charge transfers occurring within the active site, 4→5, 6→7, and 7→1, is triggered by an asymmetric charge distribution. This pendulum-like sequence is consistent with the electrostatic field directing protons from E286 towards propionate D of *heme a3*, near a putative PLS, and to the BNC, respectively before and after electron transfer from *heme a* to *heme a3*, as suggested by molecular simulations showing alternate distributions and polarizations of water in the active site [11]. Furthermore, recent experimental evidence indicates that reloading of the PLS occurs concurrently with internal electron transfer [15,18], consistent with our PLS reloading in [0|1] state 4. Proton pumping occurs in [1|1] state 2 after reprotonation of E286 which, by saturating the positive charge of the active-site region, triggers proton expulsion from the PLS. Fig. 3 explains why the PLS cannot be reloaded in the [1|1] state: if this occurred, the enzyme would cycle through 1→2→3→1…, pumping protons without any energy input.

The charge transfer steps depicted in Fig. 3 are exergonic. The activation of vectorial protons results from changes in the total charge and its distribution in the active-site region, starting from [0|1] state 4, where the proton affinity of the PLS is highest. Following reloading from E286 (transition 4→5), the proton affinity of the PLS decreases as a consequence of electron and chemical proton transfer to the BNC and of reloading E286, to reach a minimum in [1|1] state 2, when the activated proton is expelled. Reciprocally, the redox potential of both hemes depends on the protonation state of the PLS. However, the consequences of this coupling are inherently asymmetric: oxygen reduction may occur even if the PLS is never deprotonated (with a short-circuit at 2→6 resulting in the decoupling of redox activity and proton pumping), whereas proton pumping cannot occur without oxygen reduction.

A complete molecular mechanism identifying not only equilibrium properties but also kinetic gates required to guarantee the directionality of vectorial proton movement lies beyond the scope of this work. In particular, such a description will require

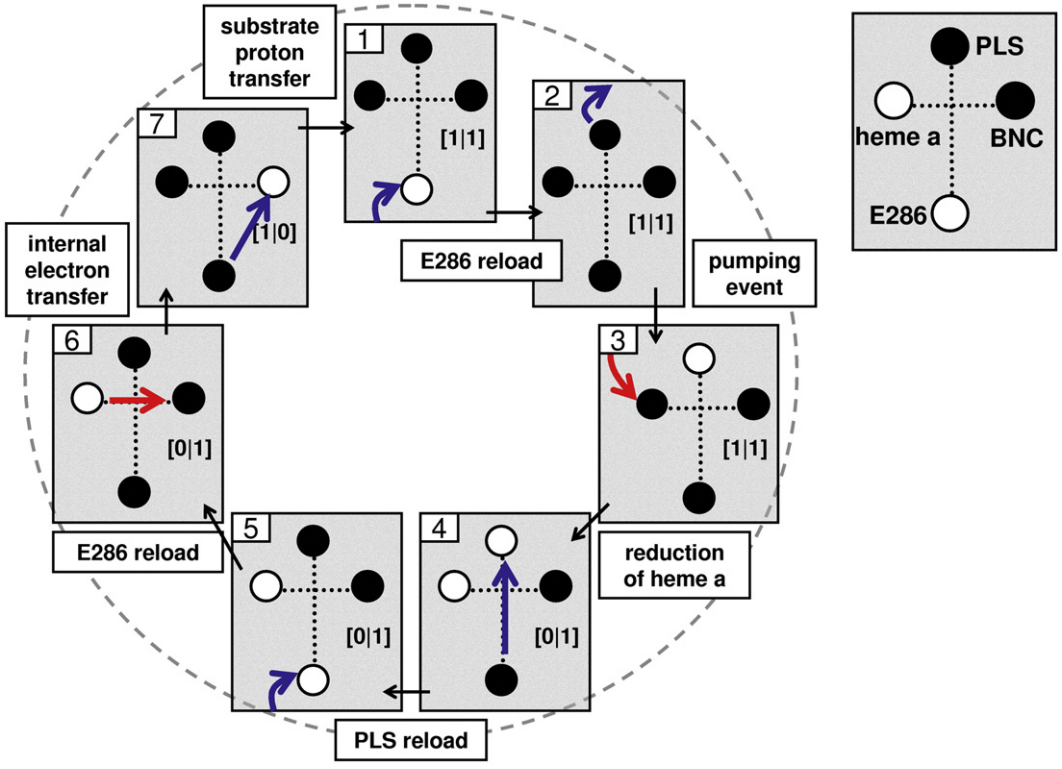

Fig. 3. Recurring sequence of electron and proton transfer events. The cross's apexes correspond to *heme a* (left), the BNC (right), the PLS (top), and E286 (bottom). Open and full circles denote unprotonated and protonated states of E286 and the PLS, and neutral and positively charged states of *heme a* and the BNC. Red and blue arrows denote electron and proton transfer events, respectively.

Table 1
Calculated pK_a of E286 in each catalytic state of the proposed catalytic mechanism (Fig. 2)

State	Charge	E286 pK_a			
		Wild-type	N207D	N139D	G204D
A	[0|1]	9.6 (0.4)	11.5 (0.4)	11.9 (0.5)	12.6 (0.4)
F	[1|1]	8.0 (0.4)	9.8 (0.4)	10.2 (0.5)	11.0 (0.4)
F_M	[0|1]	10.1 (0.3)	12.0 (0.4)	12.3 (0.5)	13.2 (0.4)
F_R	[1|0]	10.6 (0.4)	12.5 (0.4)	12.8 (0.3)	13.6 (0.5)
O	[1|1]	8.1 (0.5)	9.9 (0.5)	10.4 (0.4)	11.1 (0.4)
O_M	[0|1]	10.1 (0.6)	11.9 (0.6)	12.3 (0.6)	13.1 (0.6)
O_R	[1|0]	9.9 (0.6)	11.8 (0.6)	12.2 (0.6)	12.9 (0.6)
E	[1|1]	7.2 (0.6)	9.0 (0.6)	9.4 (0.6)	10.2 (0.6)
E_M	[0|1]	9.3 (0.6)	11.1 (0.6)	11.5 (0.6)	12.4 (0.6)
E_R	[1|0]	10.1 (0.6)	11.9 (0.7)	12.3 (0.6)	13.1 (0.6)
MV	[1|1]	7.5 (0.6)	9.4 (0.6)	9.7 (0.6)	10.6 (0.6)
Average E286 pK_a					
	[0|1]	9.9 (0.3)	11.8 (0.5)	12.2 (0.5)	13.0 (0.5)
	[1|0]	10.2 (0.5)	12.1 (0.5)	12.4 (0.6)	13.2 (0.6)
	[1|1]	7.7 (0.5)	9.6 (0.6)	10.0 (0.5)	10.8 (0.5)

States P_M and P_R were not included in the calculation because they are not accompanied by proton uptake and do not involve deprotonation of E286 [17,25,46]. Error bars, calculated as standard deviations, are indicated in parentheses. The average pK_a of E286 in [0|1], [1|0], and [1|1] charge states are shown at the bottom.

more definitive information on the identity of the PLS than is currently available. Nevertheless, the sequence of proton and electron transfer steps offers implications to the kinetic control of proton pumping. One such implication is that electron delivery to *heme a* in the [1|1] state must be slower than both (a) the reprotonation of E286 from the D-channel (i.e., transition 1→2) and (b) the expulsion of H^+ from the PLS (transition 2→3). If (a) fails, then transition 1→5 takes place and short-circuits the pump; if (b) fails, then 2→6 occurs. In both cases, pumping fails. This requirement is consistent with the observation that electron transfer from Cu_A to Fe_a is very slow [15].

In addition, the pumping cycle depicted in Fig. 3 also suggests three steps at which kinetic gating might be required to prevent proton backflow. First, kinetic barriers are in principle required to prevent protonation of the PLS from the exit (top) side in state 4, where the PLS is deprotonated and its proton affinity is maximal. Second, reloading of E286 from the D-channel (transition 1→2) may need to be fast enough to avoid the backflow of an activated proton from the PLS to E286 in state 1, which would bypass the pumping event via 1→3. Accordingly, slow proton uptake has been proposed as a possible explanation for the decoupling of proton pumping from redox activity resulting from single-point mutations in the D-channel [27]. Third, kinetic gating may be needed to ensure that chemical protons are taken up from E286 (step 7→1) rather than from the PLS (short-circuit 7→3). Finally, we note that the high pK_a of E286 throughout the catalytic cycle of the enzyme (see below) eliminates the possibility of its proton leaking back via the D-channel.

4. Validation of the proposed mechanism

Our model rests on the control of vectorial proton transfer by long-range electrostatic interactions in a recurring sequence of electron and proton transfer steps occurring in the active site. In this process, E286 plays a vital role by relaying most chemical and pumped protons. This role requires that its pK_a be high enough to guarantee reprotonation from the D-channel and low enough to relay this proton on to the PLS and the BNC. We calculated the pK_a of E286 to gauge its ability to deliver chemical and vectorial protons throughout the catalytic cycle, successively in the wild-type enzyme and in three single-point mutants in which pumping and/or redox activity are compromised. The results of continuum electrostatic calculations are shown in Table 1.

4.1. Wild-type enzyme

Consistent with spectroscopic measurements [28] and previous electrostatic calculations [29], our results indicate that E286

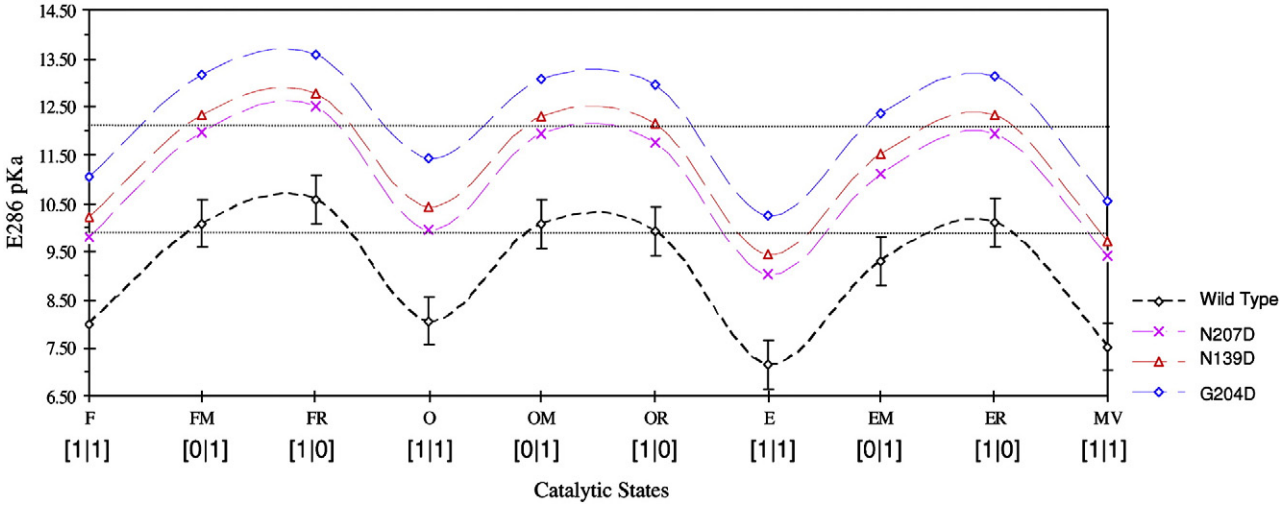

Fig. 4. pK_a of E286 in successive catalytic steps in the wild-type enzyme (black) and in single-point mutants G204D (blue), N207D (red), and N139D (pink). Approximate average pK_a of E286 in proton-delivery states [0|1] and [1|0] are shown as dotted lines for the wild-type enzyme and decoupled N139D and N207D mutants, respectively.

is protonated most of the time. The non-polar environment favors the neutral form of the carboxylic acid over the carboxylate form, so that the latter only exists transiently. Throughout the catalytic cycle, its pK_a alternates between approximately 8 and 10 depending on the total charge of the active site (Table 1). In [1|1] states F, O, E, and MV, the pK_a of E286 lies between 7.2 and 8.1, with a mean of 7.7±0.5. This result is consistent with the value of 8.3 measured for a CO adduct of the two-electron-reduced, or mixed-valence (MV) state of the enzyme [30]. In [0|1] states A, F_M, O_M, and E_M, the pK_a of E286 is in the range 9.3–10.1, with an average of 9.9±0.3, in good agreement with the values of 9.7 and 9.4 measured for the fully-reduced CO adduct (FR-CO), which is also a [0|1] state [27, 30]. At 10.2±0.6, the average pK_a of E286 in [1|0] states F_R, O_R, and E_R is essentially identical to that of [0|1] states. Thus, consistently with the recurring mechanism proposed above, the proton affinity of E286 undergoes reproducible fluctuations throughout the reductive phase of the catalytic cycle (O through MV), alternating between a higher value in proton-relay states [0|1] and [1|0], and a lower value in proton-pumping state [1|1] (Fig. 4). These periodic fluctuations support a pumping mechanism driven by recurrent changes in the charge state of the active site. More specifically, these results support electrostatic control of proton pumping, whereby the uptake and release of vectorial protons by the PLS are driven by the alternating sequence of charge states, in a way that is qualitatively (but not necessarily quantitatively) consistent with the pK_a fluctuations of E286, with a high proton affinity in [0|1] and [1|0] states, and a low proton affinity in [1|1] states.

4.2. N207D and N139D mutants

Asparagines 139 and 207 are located approximately 20 Å away from E286 in the D-channel (see Fig. 1). Both N139D and N207D mutants exhibit a decoupled phenotype whereby oxygen chemistry proceeds but not proton pumping [31,32]. This phenotype was attributed to changes in the pK_a of E286. Time-resolved spectroscopy showed that the pK_a of E286 increases by 1.6, from 9.4 for the [1|0] $P_R \rightarrow F$ transition in the wild-type, to ≈11 in the N139D mutant [27]. Accordingly, we find that, although the same oscillating pattern is observed, the pK_a of E286 is systematically higher in the N207D and N139D mutants than in the wild-type enzyme, respectively by 1.9 and 2.2 on average (Table 1, Fig. 4). This systematic pK_a upshift results from the introduction of an anionic charge in the D-channel, which further stabilizes the protonated form of E286 relative to its anionic form.

4.3. G204D mutant

In the G204D mutant, both pumping and redox activity are compromised, the latter dropping within 2% of that of the wild-type enzyme [33]. Like N139D and N207D, this point mutation increases the proton affinity of E286 compared to the wild-type. However, the closer proximity of residue 204 (16 Å away; see Fig. 1) results in a larger pK_a upshift. Specifically, the average pK_a of E286 shifts by 3, oscillating between 10.8 in [1|1] states and 13.2 in [1|0] states (Table 1, Fig. 4).

Thus, consistently with previous studies [27,31,33], our results indicate that the introduction of an anionic residue in the D-channel increases the proton affinity of E286 and suggest that the phenotypes of N139D, N207D, and G204D mutants are due to systematic pK_a upshifts. These findings contrast with a recent continuum electrostatic study of *P. denitrificans* C*c*O, in which N131D (analogous to N139D in *R. sphaeroides* C*c*O) had no influence on the pK_a of E278 (E286) [34]. While the two studies differ significantly in the charge state of the enzyme and the distribution of atomic point charges, as well as in dielectric constants and dielectric boundaries, our results are supported by experimental data in terms of absolute pK_a and pK_a shifts, both in wild-type and mutant enzymes [27,31,33].

The decoupled phenotype of N139D and N207D results from the inability of E286 to reload the PLS. In both mutants, the proton affinity of E286 in [0|1] states is too high for transition $4 \rightarrow 5$ to occur (Fig. 3). Instead, $4 \rightarrow 6$ takes place upon reprotonation of the PLS from the exit channel: the pump slips, cancelling the effect of PLS deprotonation in the $2 \rightarrow 3$ transition. Effectively, the cycle is short-circuited at $2 \rightarrow 6$, decoupling redox chemistry (steps 6 through 2) from proton pumping (Fig. 3). This mechanism implies that the pK_a of the PLS in the [0|1] state is near 11, intermediate between that of E286 in the wild-type and in the decoupled mutants (Fig. 4). This estimate is in quantitative agreement with the value of 10.7 calculated for a reduced *heme a* state equivalent to our [0|1] state [35].

The high pK_a of E286, which lies between 12.5 and 13.5 in both proton-delivery states [0|1] and [1|0], explains the G204D phenotype by the inability of E286 to deliver not only vectorial protons but also chemical protons. This rationale places a lower bound of p$K_a \sim 13$ for the high proton affinity intermediates of the active site, since this value separates the pK_a of E286 in the [1|0] states of the G204D mutant from those of redox-active mutants N139D and N207D (Fig. 4). Residual redox activity in the G204D mutant [33] may be explained by the lowest pK_a of E286, which is approximately 13 in O_R and E_R states (Table 1). In the G204D mutant, E286 is not readily deprotonated. Intermediate 5 disappears and intermediate 1 is virtually eliminated, stalling redox activity (see Fig. 3).

5. Conclusions

Our proposed scheme is based on the breakdown of each of the four observable transitions in the catalytic cycle of C*c*O into a recurring sequence of three electrostatic states which repeats itself identically four times per turnover, regardless of the chemistry taking place in the BNC. By successively regulating the distribution of vectorial and substrate protons and the expulsion of a pumped proton, the alternation of these electrostatic states ensures the stoichiometric coupling of proton pumping to redox chemistry. The repetition of this scheme provides a simple and robust principle controling vectorial proton translocation throughout the catalytic cycle. Thus, this theoretical framework represents a significant step towards a complete description of the pumping mechanism in C*c*O. As noted in the text, our model is consistent with a vast body of experimental work. By offering a detailed description of the catalytic cycle, this work opens the way to

systematic investigations of the molecular basis of charge transfer in and out of the active site of the enzyme. As a first step, electrostatic calculations support our proposed mechanism and suggest that the decoupled and inactive phenotypes induced by ionic single-point mutations in the D-channel result from compromised delivery of vectorial and chemical protons.

6. Computational method

The initial structure of the enzyme was taken from Ref. [36]. The distribution of charge in the BNC was modeled with quantum calculations, the charge distribution of oxidized *heme a* was taken from Olkhova et al. [34], and the rest of the protein was described by the CHARMM22 force field [37].

6.1. Quantum calculations

The reaction intermediates were modeled by optimization of a reduced model of the BNC (see Supplementary material) using unrestricted hybrid-DFT (U-B3LYP) calculations [38]. All heavy atoms were described by SBKJC effective core potentials and a double-ζ basis for valence electrons [39, 40]. Atomic point charges were obtained by fit to the electrostatic potential calculated at the 6-31G*/U-B3LYP level of theory. These charges were rescaled to embed propionates A and D and the *heme a3* side chains (see Supplementary material). All DFT calculations were performed with version 4.6 of NWChem [41].

6.2. Protonation states

We assume that the protonation state of residues not directly involved in the redox chemistry does not change throughout the catalytic cycle, with the exception of E286 and the PLS. We consider the propionate groups of both *heme a* and *heme a3* to be deprotonated, since their carboxylate groups are stabilized by interactions with Arg side chains and with the protein backbone [29,36]. Based on recent calculations [42], H333, H334, and H284, which coordinate Cu_B, remain neutral throughout the catalytic cycle. To determine the protonation state of the three Asp residues introduced in the D-channel by single-point mutations, we calculated the pK_a shift of these residues relative to their standard acidity in water (i.e., 3.9), with E286 protonated. Results for N139D, N207D, and G204D were <1, <2, and ~ 3, respectively, indicating that these residues are anionic. Because the identity of the PLS is unknown, the effect of changes in the protonation state of the PLS on the pK_a of E286 could not be included in the electrostatic calculations.

6.3. Continuum electrostatic calculations

The pK_a shift calculations were performed with the PBEQ module [43] of CHARMM [44] using atomic radii optimized for continuum electrostatic calculations [45]. We assigned dielectric constants of 2 to the 45-Å-thick membrane slab, 80 to the solvent, and 5 to the protein interior. The salt concentration was set to 150 mM. The D-channel was embedded in a cylinder of 8 Å radius and 24 Å height within which the dielectric constant of the cavity was set to 80. No explicit water molecules other than those produced by the redox chemistry were included in the PBEQ calculation. The Poisson–Boltzmann equation was solved numerically by finite-difference on a coarse grid (0.60 Å mesh size) focused on regions of interest up to a 0.30-Å mesh size. The pK_a values reported in Table 1 represent an average of the values calculated for 100 snapshots selected randomly from five independent 2.5-ns molecular dynamics trajectories to take into account conformational fluctuations in the D-channel. Additional calculations were performed to ensure that the pK_a of E286 is independent of the redox state of Cu_A: upon Cu_A reduction, it increases by 0.4 (data not shown), which is within the accuracy of the method.

6.4. Molecular dynamics

Subunit I of the enzyme with a 15-Å-radius hemispherical cap of TIP3P water at the entrance of the D-channel was simulated at 300 K using Langevin dynamics. The initial side-chain conformations of N139D, N207D, and G204D mutants were created manually, energy-minimized, and subjected to 500 ps of equilibration at 300 K before production. During dynamics, only the residues and water molecules comprised in a cylinder of 24 Å height and 8 Å radius centered on the axis of the D-channel, including D132 and E286, were allowed to move.

Acknowledgements

We thank Robert B. Gennis for the insightful discussions and Nilmadhab Chakrabarti for his advice on the electrostatic calculations. This work was supported by Canadian Institute for Health Research operating grant MOP43949. R.P. is a Canada Research Chair.

Appendix A. Supplementary data

Supplementary data associated with this article can be found, in the online version, at doi:10.1016/j.bbabio.2007.11.010.

References

[1] M. Wikström, M.I. Verkhovsky, Towards the mechanism of proton pumping by the haem-copper oxidases, Biochim. Biophys. Acta 1757 (2006) 1047–1051.
[2] G. Brändén, R.B. Gennis, P. Brzezinski, Transmembrane proton translocation by cytochrome *c* oxidase, Biochim. Biophys. Acta 1757 (2006) 1052–1063.
[3] P. Brzezinski, P. Ädleroth, Design principles of proton-pumping haem-copper oxidases, Curr. Opin. Struct. Biol. 16 (2006) 465–472.
[4] M. Wikström, Proton pump coupled to cytochrome *c* oxidase in mitochondria, Nature 266 (1977) 271–273.
[5] A.A. Konstantinov, S. Siletsky, D. Mitchell, A. Kaulen, R.B. Gennis, The roles of the two proton input channels in cytochrome *c* oxidase from *Rhodobacter sphaeroides* probed by the effects of site-directed mutations on time-resolved electrogenic intraprotein proton transfer, Proc. Natl. Acad. Sci. U. S. A. 94 (1997) 9085–9090.
[6] P. Brzezinski, P. Ädleroth, Pathways of proton transfer in cytochrome *c* oxidase, J. Bioenerg. Biomembranes 30 (1998) 99–107.
[7] R.M. Nyquist, D. Heitbrink, C. Bolwien, R.B. Gennis, J. Heberle, Direct observation of protonation reactions during the catalytic cycle of cytochrome *c* oxidase, Proc. Natl. Acad. Sci. U. S. A. 100 (2003) 8715–8720.

[8] H. Michel, The mechanism of proton pumping by cytochrome *c* oxidase, Proc. Natl. Acad. Sci. U. S. A. 95 (1998) 12819–12824.
[9] S. Riistama, G. Hummer, A. Puustinen, R.B. Dyer, W.H. Woodruff, M. Wikström, Bound water in the proton translocation mechanism of haem-copper oxidases, FEBS Lett. 414 (1997) 275–280.
[10] S.A. Seibold, D.A. Mills, S. Ferguson-Miller, R.I. Cuckier, Water chain formation and possible proton pumping routes in *Rhodobacter sphaeroides* cytochrome *c* oxidase: a molecular dynamics comparison of the wild type and R481K mutant, Biochemistry 44 (2005) 10475–10485.
[11] M. Wikström, M.I. Verkhovsky, G. Hummer, Water-gated mechanism of proton translocation by cytochrome *c* oxidase, Biochim. Biophys. Acta 1604 (2003) 61–65.
[12] P.R. Rich, Towards an understanding of the chemistry of oxygen reduction and proton translocation in the iron–copper respiratory oxidases, Aust. J. Plant Physiol. 22 (1995) 479–486.
[13] M. Iwaki, A. Puustinen, M. Wikström, P.R. Rich, Structural and chemical changes of the PM intermediate of *Paracoccus denitrificans* cytochrome *c* oxidase revealed by IR spectroscopy with labeled tyrosines and histidine, Biochemistry 45 (2006) 10873–10885.
[14] M. Wikström, C. Ribacka, M. Molin, L. Laakkonen, M.I. Verkhovsky, A. Puustinen, Gating of proton and water transfer in the respiratory enzyme cytochrome *c* oxidase, Proc. Natl. Acad. Sci. U. S. A. 102 (2005) 10478.
[15] I. Belevich, D. Bloch, N. Belevich, M. Wikström, M.I. Verkhovsky, Exploring the proton pump mechanism of cytochrome *c* oxidase in real time, Proc. Natl. Acad. Sci. U. S. A. 104 (2007) 2685–2690.
[16] H. Michel, J. Behr, A. Harrenga, A.C. Kannt, Cytochrome *c* oxidase: structure and spectroscopy, Annu. Rev. Biophys. Biomol. Struct. 27 (1998) 329–356.
[17] K. Faxén, G. Gilderson, P. Ädelroth, P. Brzezinski, A mechanistic principle for proton pumping by cytochrome *c* oxidase, Nature 437 (2005) 286–289.
[18] I. Belevich, M.I. Verkhovsky, M. Wikström, Proton-coupled electron transfer drives the proton pump of cytochrome *c* oxidase, Nature 440 (2006) 829–832.
[19] M. Wikström, M.I. Verkhovsky, Mechanism and energetics of proton translocation by the respiratory heme-copper oxidases, Biochim. Biophys. Acta 1767 (2007) 1200–1214.
[20] M. Wikström, Cytochrome *c* oxidase: 25 years of the elusive proton pump, Biochim. Biophys. Acta 1655 (2004) 241–247.
[21] S. Siletsky, D. Han, S. Brand, J.E. Morgan, M. Fabian, L. Geren, F. Millett, B. Durham, A.A. Konstantinov, R.B. Gennis, Single-electron photoreduction of the P_M intermediate of cytochrome *c* oxidase, Biochim. Biophys. Acta 1757 (2006) 1122–1132.
[22] M.I. Verkhovsky, I. Belevich, D. Bloch, M. Wikström, Elementary steps of proton translocation in the catalytic cycle of cytochrome *c* oxidase, Biochim. Biophys. Acta 1757 (2006) 401–407.
[23] D.A. Proshlyakov, M.A. Pressler, C. DeMaso, J.F. Leykam, D.L. DeWitt, G.T. Babcock, Oxygen activation and reduction in respiration: involvement of redox-active tyrosine 244, Science 290 (2000) 1588–1591.
[24] G.T. Babcock, How oxygen is activated and reduced in respiration, Proc. Natl. Acad. Sci. U. S. A. 96 (1999) 12971–12973.
[25] M. Brändén, H. Sigurdson, A. Namslauer, R.B. Gennis, P. Ädelroth, P. Brzezinski, On the role of the K-proton transfer pathway in cytochrome *c* oxidase, Proc. Natl. Acad. Sci. U. S. A. 98 (2001) 5013–5018.
[26] P.E.M. Siegbahn, M.R.A. Blomberg, M.L. Blomberg, Theoretical study of the energetics of proton pumping and oxygen reduction in cytochrome oxidase, J. Phys. Chem., B 107 (2003) 10946–10955.
[27] A. Namslauer, A.S. Pawate, R.B. Gennis, P. Brzezinski, Redox-coupled proton translocation in biological systems: proton shuttling in cytochrome *c* oxidase, Proc. Natl. Acad. Sci. U. S. A. 100 (2003) 15543–15547.
[28] A. Puustinen, J.A. Bailey, R.B. Dyer, S.L. Mecklenburg, M. Wikström, W.H. Woodruff, Fourier transform infrared evidence for connectivity between Cu_B and glutamic acid 286 in cytochrome bo_3 from *E. coli*, Biochemistry 36 (1997) 13195–13200.
[29] A.C. Kannt, R.D. Lancaster, H. Michel, The coupling of electron transfer and proton translocation: electrostatic calculations on *Paracoccus denitrificans* cytochrome *c* oxidase, Biophys. J. 74 (1998) 708–721.
[30] B.H. McMahon, M. Fabian, F. Tomson, T.P. Causgrove, J.A. Bailey, F.N. Rein, R.B. Dyer, G. Palmer, R.B. Gennis, W.H. Woodruff, FTIR study of internal proton transfer reactions linked to inter-heme electron transfer in bovine cytochrome *c* oxidase, Biochim. Biophys. Acta 1655 (2004) 321–331.
[31] D. Han, A. Namslauer, A.S. Pawate, J.E. Morgan, S. Nagy, A.S. Vakkasoglu, P. Brzezinski, R.B. Gennis, Replacing Asn207 by aspartate at the neck of the D-channel in the aa_3-type cytochrome *c* oxidase from *Rhodobacter sphaeroides* results in decoupling the proton pump, Biochemistry 45 (2006) 14064–14074.
[32] A.S. Pawate, J. Morgan, A. Namslauer, D. Mills, P. Brzezinski, S. Ferguson-Miller, R.B. Gennis, A mutation in subunit I of cytochrome *c* oxidase from *Rhodobacter sphaeroides* results in an increase in steady state activity but completely eliminates proton pumping, Biochemistry 41 (2002) 13417–13423.
[33] D. Han, J.E. Morgan, R.B. Gennis, G204D a mutation that blocks the proton conducting D-channel of the aa_3-type cytochrome *c* oxidase from *Rhodobacter sphaeroides*, Biochemistry 44 (2005) 12767–12774.
[34] E. Olkhova, V. Helms, H. Michel, Titration behavior of residues at the entrance of the D-pathway of cytochrome *c* oxidase from *Paracoccus denitrificans* investigated by continuum electrostatic calculations, Biophys. J. 89 (2005) 2324–2331.
[35] P.E.M. Siegbahn, M.R.A. Blomberg, Energy diagrams and mechanisms for proton pumping in cytochrome *c* oxidase, Biochim. Biophys. Acta 1767 (2007) 1143–1156.
[36] M. Svensson-Ek, J. Abramson, G. Larsson, S. Törnroth, P. Brzezinski, S. Iwata, The X-ray crystal structures of wild-type and EQ(I-286) mutant cytochrome *c* oxidases from *Rhodobacter sphaeroides*, J. Mol. Biol. 321 (2002) 329–339.
[37] A.D. MacKerell, D. Bashford, M. Bellott, R.L. Dunbrack, J.D. Evanseck, M.J. Field, S. Fischer, J. Gao, H. Guo, S. Ha, D. Joseph-McCarthy, L. Kuchnir, K. Kuczera, F.T.K. Lau, C. Mattos, S. Michnick, T. Ngo, D.T. Nguyen, B. Prodhom, W.E. Reiher, B. Roux, M. Schlenkrich, J.C. Smith, R. Stote, J. Straub, M. Watanabe, J. Wiorkiewicz-Kuczera, D. Yin, M. Karplus, All-atom empirical potential for molecular modeling and dynamics studies of proteins, J. Phys. Chem., B 102 (1998) 3586–3616.
[38] P.J. Stevens, J.F. Devlin, C.F. Chabalowski, M.J. Frisch, Ab Initio calculations of vibrational absorption and circular dichroism spectra using SCF, MP2, and density functional theory force fields, J. Phys. Chem. 98 (1994) 11623.
[39] W.J. Stevens, H. Bash, M. Krauss, Compact effective potentials and efficient shared-exponent basis sets for the first- and second-row atoms, J. Chem. Phys. 81 (1984) 6026.
[40] W.J. Stevens, M. Krauss, H. Bash, P.G. Jasien, Relativistic compact effective potentials and efficient, shared-exponent basis sets for the third-, fourth-, and fifth-row atoms, Can. J. Chem. 70 (1992) 612.
[41] T.P. Straatsma, E. Aprà, T.L. Windus, E.J. Bylaska, W. de Jong, S. Hirata, M. Valiev, M. Hackler, L. Pollack, R. Harrison, M. Dupuis, D.M.A. Smith, J. Nieplocha, V. Tipparaju, M. Krishnan, A.A. Auer, E. Brown, G. Cisneros, G. Fann, H. Früchtl, J. Garza, K. Hirao, R. Kendall, J. Nichols, K. Tsemekhman, K. Wolinski, J. Anchell, D. Bernholdt, P. Borowski, T. Clark, D. Clerc, H. Dachsel, M. Deegan, K. Dyall, D. Elwood, E. Glendening, M. Gutowski, A. Hess, J. Jaffe, B. Johnson, J. Ju, R. Kobayashi, R. Kutteh, Z. Lin, R. Littlefield, X. Long, B. Meng, T. Nakajima, S. Niu, M. Rosing, G. Sandrone, M. Stave, H. Taylor, G. Thomas, J. van Lenthe, A. Wong, Z. Zhang, *NWChem, A Computational Chemistry Package for Parallel Computers*, Version 4.6, Pacific Northwest National Laboratory, Richland, Washington 99352–0999, USA. (2004)
R.A. Kendall, E. Aprà, D.E. Bernholdt, E.J. Bylaska, M. Dupuis, G.I. Fann, R.J. Harrison, J. Ju, J.A. Nichols, J. Nieplocha, T.P. Straatsma, T.L. Windus, A.T. Wong, High Performance Computational Chemistry: an Overview of NWChem a Distributed Parallel Application, Computer Phys. Comm. 128 (2000) 260–283.
[42] E. Fadda, N. Chakrabarti, R. Pomès, Acidity of a Cu-bound histidine in the binuclear center of cytochrome *c* oxidase, J. Phys. Chem., B 109 (2005) 22629–22640.
[43] W. Im, D. Beglov, B. Roux, Continuum solvation model electrostatic forces from numerical solutions to the Poisson Boltzmann equation, Comp. Phys. Comm. 111 (1998) 59–75.
[44] B.R. Brooks, R.E. Bruccoleri, B.D. Olafson, D.J. States, S. Swaminathan, M. Karplus, CHARMM — a program for macromolecular energy, minimization, and dynamics calculations, J. Comput. Chem. 4 (1983) 187–217.
[45] M. Nina, W. Im, B. Roux, Optimized atomic radii for protein continuum electrostatic solvation forces, Biophys. Chem. 78 (1999) 89–96.
[46] M. Wikström, M.I. Verkhovsky, Proton translocation by cytochrome *c* oxidase in different phases of the catalytic cycle, Biochim. Biophys. Acta, Bioenerg. 1555 (2002) 128–132.